Chain Stiffness of a High Molecular Weight Polyguanidine Prepared by Living Polymerization

Mu-Ping Nieh, Andrew A. Goodwin, Jennifer R. Stewart, Bruce M. Novak, and Dave A. Hoagland*

Department of Polymer Science & Engineering and the Materials Research Science and Engineering Center, University of Massachusetts, Amherst, Massachusetts 01003

Received December 10, 1997
Revised Manuscript Received March 17, 1998

Introduction. From both theoretical and practical perspectives, soluble polymers with high backbone rigidity comprise an enticing, but elusive, class of materials. Biological sources provide the most important examples, including DNA and a few polysaccharides.[1−5] Nearly all synthetic polymers of this type are prepared via step-growth methodologies, and as a consequence, are characterized by low molecular weight and large polydispersities. Our desire to remedy these deficiencies has led us to develop living chain-growth routes to stiff polymers, with rigidity to be derived principally from restricted rotations about main-chain bonds. Chain-growth mechanisms facilitate polymerization to high molecular weight, while livingness promotes uniformity in molecular weight distribution. Examples of the living chain-growth approach include polyisocyanides,[6] polyisocyanates,[7] and more recently, polyguanidines.[8] By combining in the polyguanidine the separate structural characteristics believed responsible for the stiffness of polyisocyanides and polyisocyanates, we expect to make a chain that is stiffer than either. Herein, we report light-scattering studies that confirm the stiff-chain characteristics of a representative poly(guanidine), poly[(*R*/*S*)-*N*-(1-phenylethyl)-*N*′-methylcarbodiimide], poly-**I**.[9]

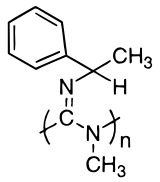

Poly-**I**

Experimental Section. For a set of poly-**I** samples varying only in average molecular weight ($10^5 < M_w < 2.8 \times 10^6$), the radius of gyration R_g was measured as a function of molecular weight M using tandem size exclusion chromatography−light scattering (SEC−LS). The SEC−LS setup employed a Hewlett-Packard 1050 series liquid chromatography pump, a Wyatt Technologies Dawn DSP-F light-scattering instrument operated at 632.5 nm and equipped with a K5 flow cell, and a Wyatt Technologies Optilab 903 refractive index detector outfitted with a P-10 flow cell thermostated at 25 °C. During SEC−LS, polymer samples dissolved in HPLC grade THF were fractionated during flow at 1.0 mL/min through a set of three size exclusion columns (PLGel, Mixed C, 5 μm particle size, Polymer Laboratories). The same experimental sequence confirmed the narrowness of the molecular weight distributions.

An ALV-5000 goniometer/correlator in conjunction with a 3 W Coherent argon ion laser (set to 30 mW) permitted static and dynamic light-scattering (S-DLS) experiments to be performed simultaneously on unfractionated solution samples at 514 nm; investigations with the instrument focused on a single poly-**I** ($M_w = 7.8 \times 10^5$; $M_w/M_n = 1.28$). The sample was dissolved in THF (0.1, 0.2, 0.3, 0.4, and 0.5 mg/mL), and the resulting solutions were then filtered through 0.5 μm filters (Millex SR, Millipore) into 1.0 cm diameter scattering cells. The DLS data were interpreted by the method of cumulants; given the near single exponential character of the correlation function, the data could equally well have been interpreted by another method. The anisotropy factor δ, potentially significant for short and stiff chains,[10] was determined by comparing polarized and depolarized static scattered intensities. The maximum correction due to nonzero δ was found to be ~3% in M; given the small magnitude of the effect, chain anisotropy was ignored in subsequent data analyses.

Results and Discussion. The Benoit−Doty formula[11] expresses R_g^2 of a Kratky−Porod wormlike chain[12] in terms of two model parameters, the persistence length L_p and the contour length L,

$$R_g^2 = L^2 f(L_p/L) \tag{1}$$

where the dimensionless function f can be written

$$f(x) = \frac{1}{3}x - x^2 + 2x^3 - 2x^4[1 - \exp(-1/x)] \tag{2}$$

In the asymptotic limits $x \to 0$ and $x \to \infty$, these equations recover the usual molecular weight−size relationships for Gaussian and rodlike chains, respectively, and in these limits, R_g^2 can be fully characterized by a single parameter, either $LL_p(x \to 0)$ or $L(x \to \infty)$. The Kuhn segment length L_k, an alternative measure of the stiffness based on a freely jointed chain description, is exactly $2L_p$ in the Gaussian limit. Experimentally, M is a more accessible variable than L; when M replaces L as a measure of chain length, the second parameter of the wormlike chain model becomes the mass-per-length M_L ($=M/L$) and x can be represented by L_pM_L/M; x^{-1} is the number of persistence lengths comprising the chain backbone.

Light-scattering data for $R_g(M)$ have often been fit to the Benoit−Doty formula to obtain L_p and M_L.[13,14] For $x \gg 1$, a plot of R_g^2/M^2 vs M best manifests the quality of such a fit, but for $x \leq 1$, a plot of R_g^2/M vs M is more revealing. Displayed in the latter format, the Benoit−Doty formula predicts ordinate values at low M that grow linearly with slope $1/(12M_L^2)$, while at high M, the same formula predicts that the ordinate reaches a plateau of $L_p/(3M_L)$. Thus, one conceivably could obtain L_p and M_L by a graphical analysis of $R_g(M)$ data at high and low M. Unfortunately, this simple approach requires an impractically large range of M, one corresponding to $0.01 < x^{-1} < 100$. As a simpler alternative, L_p and M_L are obtained by fitting experimental data at intermediate x, preferably across the range $0.1 \leq x^{-1} \leq$

* To whom correspondence should be addressed

S0024-9297(97)01800-7 CCC: $15.00
Published on Web 04/11/1998

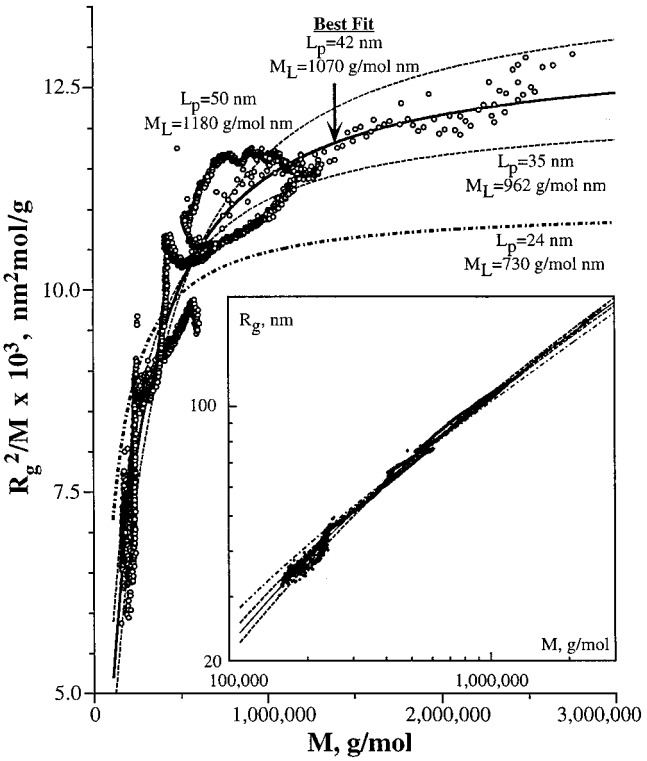

Figure 1. Comparison of $R_g(M)$ data from SEC−LS experiments with predictions of the Benoit−Doty formula. The solid curve is a two-parameter least-mean-squares fit to the data, while the two dashed curves are best fits with L_p fixed at 35 and 50 nm. In the inset, the same data and curves are shown in a log−log format.

50. The greater is the M span of these data, the greater is the confidence in the fitted values of L_p and M_L.

Figure 1 displays R_g^2/M vs M for seven different poly-**I** samples; data are shown for one SEC−LS run of each sample. Since the polydispersities are narrow, a single run produces a dense curve of 300−500 data points that extends across a limited M range. The waviness and splitting of the composite curve, covering a much larger M range, reflects measurement inconsistencies in regions where the different M distributions overlap. Most of the deviation is attributed to difficulties in selecting a consistent baseline for the leading and tailing ends of an SEC peak, regions where the refractive index and light-scattering intensities of the peak are relatively weaker. Alongside the experimental data are plotted the predictions of the Benoit−Doty formula for different values of L_p and M_L. The central solid curve corresponds to a least-mean-squares fit of the experimental data; this fit yields values for L_p and M_L of 42 nm and 1080 g/(mol nm), respectively. Adopting these values, we infer that the composite plot represents $3 < x^{-1} < 60$. The maximum deviation between best fit theory and experiment is 16% in R_g^2/M and 3% in R_g. The two dashed curves in Figure 1 correspond to the most extreme parameter values that can be considered to fit reasonably the experimental data. From these curves, we infer that 35 nm $< L_p <$ 50 nm.

The Benoit−Doty formula rigorously applies only to a monodisperse polymer sample dissolved in a Θ solvent, a condition in which excluded volume-induced chain expansion can be ignored. Because the current SEC−LS measurements are performed on chains fractionated before light-scattering analysis, polydispersity can be safely neglected. The good solvent quality of

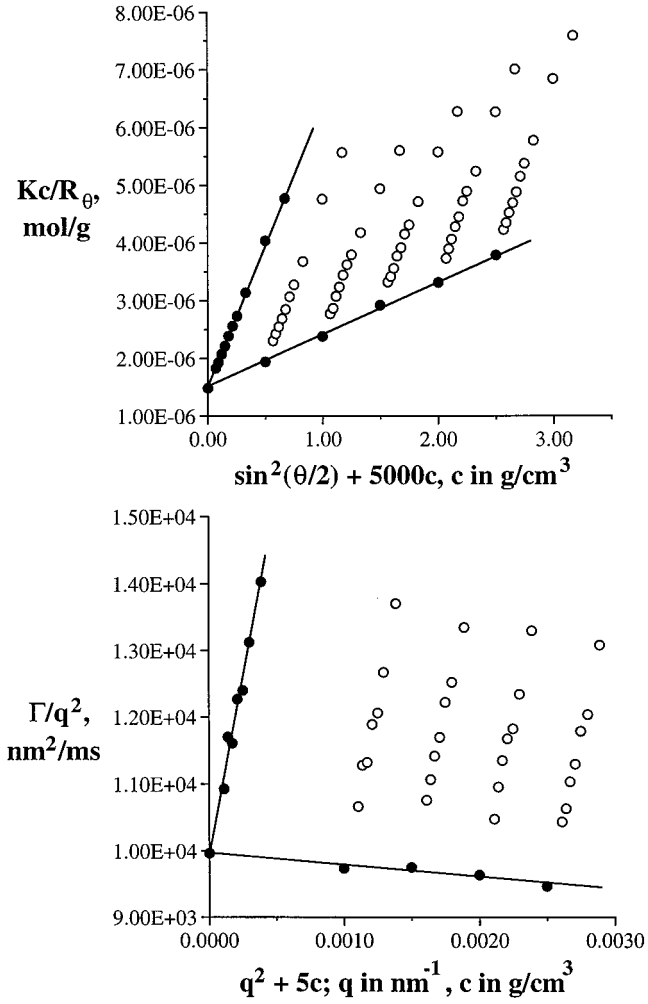

Figure 2. Static and dynamic Zimm plots from which $\langle R_g^2\rangle^{1/2}$ and $\langle 1/R_H\rangle^{-1}$ are determined. Filled data points are extrapolations.

THF for poly-**I** is a more worrisome issue. Using a wormlike pearl necklace model, Yamakawa and Stockmayer[13,15] showed that with weak excluded volume the chain expansion factor α can be written

$$\alpha^2 = 1 + K(x)z + ... \quad (3)$$

where $K(x)$ is an order unity constant and z is the excluded volume parameter,

$$z = (3/2\pi)^{3/2}(\beta/l^2)(L^{1/2}/L_k 3/2) \quad (4)$$

written in terms of the bead "excluded volume" β and bead diameter l. In the present case, l can be approximated roughly as the size of a repeat unit and β can be estimated crudely as l^3. Making these substitutions and gathering order unity constants into a prefactor C,

$$\alpha^2 \approx 1 + C(L/L_p)^{1/2}(l/L_p) \quad (5)$$

For poly-**I**, l will be a few nanometers at most. Substituting the necessary values/estimates into eq 5 while setting C to 1.0, we calculate that α deviates by only a few percent from unity in the worst case (when $M = 2.8 \times 10^6$), supporting the suggestion that solvent quality has little impact on chain dimensions across the

range of M examined. In further support of this rough analysis, Norisuye and Fujita[16] found from scattering experiments on similar wormlike polymers that excluded volume only becomes significant when x^{-1} is in excess of 100. In fact, upturns of R_g^2/M of the sort seen in Figure 1 for $M > 2 \times 10^6$ ($x^{-1} > 50$) have tentatively been identified with the onset of excluded volume effects.[14,17]

Additional methods to characterize the structure of wormlike chains include X-ray scattering, neutron scattering, and depolarized light scattering. We choose, however, to confirm our SEC−LS results by using the S-DLS method. As the S-DLS method is tedious, measurements are limited to a single poly-**I** sample of intermediate M. Yamakawa and Fujii[18] showed that the effective hydrodynamic radius R_H of a wormlike chain can be written

$$R_H^2 = L^2 F(x,d) \tag{6}$$

where d is the effective backbone diameter (made dimensionless by L_p) and F is a tabulated function. Dependence on L can be eliminated by taking the ratio of eq 1 to eq 6:

$$\frac{R_g^2}{R_H^2} = \frac{f(x)}{F(x,d)} \tag{7}$$

Static and dynamic light-scattering experiments in dilute solution yield the two z-averages, $\langle R_g^2\rangle_z^{1/2}$ and $\langle 1/R_H\rangle_z^{-1}$, respectively. SEC fractionation before a combined static/dynamic light-scattering measurement remains impractical; thus, depending on the value of the polydispersity, $f(x)$ and $F(x,d)$ may need modification before $\langle R_g^2\rangle_z^{1/2}$ and $\langle 1/R_H\rangle_z^{-1}$ are employed on the left-hand side of eq 7. After polydispersity corrections, and with d known independently, eq 7 allows an implicit determination of x. Finally, by rearranging eq 1, we obtain a second value for L_p,

$$L_p = \frac{x}{f(x)}\langle R_g^2\rangle_z^{1/2} \tag{8}$$

and thus for M_L. Schmidt[19] discusses the S-DLS evaluation of L_p in detail. In particular, he shows that corrections for polydispersity are much greater for $\langle R_g^2\rangle_z^{1/2}$ than for $\langle 1/R_H\rangle_z^{-1}$.

Values of $\langle R_g^2\rangle_z^{1/2}$ and $\langle 1/R_H\rangle_z^{-1}$ for the selected poly-**I** sample are calculated from the static and dynamic Zimm plots presented in Figure 2; the Zimm plot formalism allows consistent linear extrapolation of Kc/R_θ and Γ/q^2 to zero concentration and zero angle. (The optical constant K, polymer concentration c, Rayleigh ratio R_θ, first cumulant Γ, and scattering vector q all have their usual meanings.) From slopes and intercepts, we determine that $M_w = 6.73 \times 10^5$, $A_2 = 2.59 \times 10^{-3}$ (mol cm^3)/g^2, $\langle R_g^2\rangle_z^{1/2} = 99$ nm, and $\langle 1/R_H\rangle_z^{-1} = 39.6$ nm. Agreement of $\langle R_g^2\rangle_z^{1/2}$ with the SEC−LS values is within 3%. Although M_w compares less favorably (≈11%), most of the discrepancy can be traced to insertion into the static scattering analysis of the refractive index increment of poly-**I**/THF at 633 nm; the S-DLS experiment is performed at 514 nm, a wavelength at which the refractive index increment is unknown. Fortunately, choice of a refractive index increment does not affect the determination of the target parameter, $\langle R_g^2\rangle_z^{1/2}$.

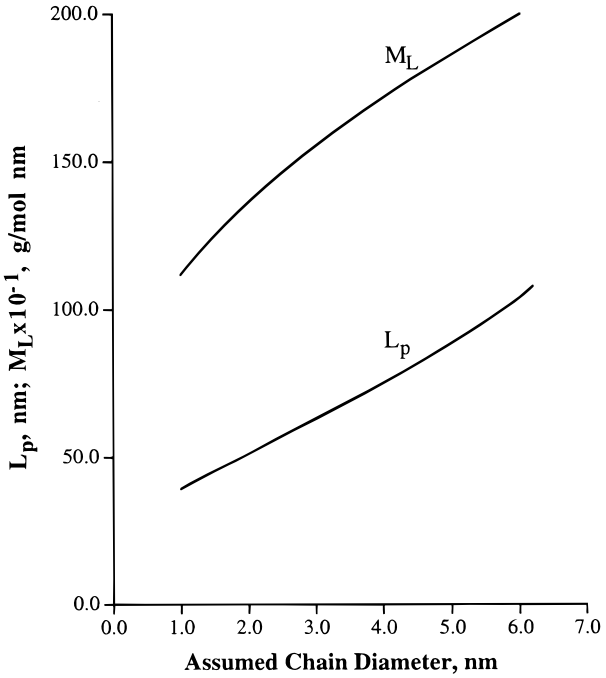

Figure 3. Dependence of L_p and M_L on the hydrodynamic diameter assumed for the poly-**I** backbone in the S−DLS analysis.

Combining $\langle R_g^2\rangle_z^{1/2}$ and $\langle 1/R_H\rangle_z^{-1}$ into a polydispersity-corrected version of eq 7, we observe that solutions for x exist only if $d < 0.0282$; this inequality limits L_p to values less than 108 nm. In the absence of better information, Tsuji, Norisuye, and Fujita[20] suggest that d be estimated from the bulk polymer density ρ

$$\rho = 4M_L/(\pi d^2 N_A) \tag{9}$$

where ρ for poly-**I** is 1.17 ± 0.025 g/cm^3.[21] From eqs 7−9, 1.5 nm, 45 nm, and 1250 g/(mol nm) are calculated, respectively, for d, L_p, and M_L, the latter values in remarkably good accord with those from SEC−LS. Figure 3 shows that the values of L_p and M_L calculated by S-DLS are relatively insensitive to the choice of d. In fact, even supposing an error in the estimated diameter by a factor of 2, the accuracy of the SLS−DLS measurement of L_p remains comparable to the one obtained by SEC−LS.

The two experimental approaches provide a consistent conclusion, that this achiral polymer is among the stiffest of soluble synthetic polymers, with $L_p = 42 \pm 8$ nm. The origins of the great stiffness are not entirely clear. The mixed chirality of the repeat units would seem to disallow the development of long range helical structure, leaving steric hindrance and electron resonance as the only major stiffening effects. If so, the stiffness in solution is extraordinary, perhaps higher than ever reported for a polymer not adopting a regular helical structure. The combination of stiffness with narrow chain length distribution should endow this polymer and its analogues with unusual and perhaps important properties.

Acknowledgment. D.A.H. and M.-P.N. wish to thank NSF-DMR for the support of our static light-scattering work and the UMass MRSEC for support of the dynamic light-scattering instrumentation. B.M.N. acknowledges the NSF-DMR, DNR, and UMass MRSEC for financial support.

References and Notes

(1) Yamakawa, H.; Fujii, M. *Macromolecules* **1974**, *7*, 128.
(2) Record, M. T., Jr.; Woodbury, C. P.; Inman R. B. *Biopolymers* **1975**, *14*, 393.
(3) Yanaki, T.; Norisuye, T.; Fujita, H. *Macromolecules* **1980**, *13*, 1462.
(4) Kashiwagi, Y.; Norisuye, T.; Fujita, H. *Macromolecules* **1981**, *14*, 1462.
(5) Sato, T.; Norisuye, T.; Fujita, H. *Macromolecules* **1984**, *17*, 2696.
(6) Deming, T. J.; Novak, B. M. *J. Am. Chem. Soc.* **1993**, *115*, 9101.
(7) Patten, T. E.; Novak, B. M. *J. Am. Chem. Soc.* **1996**, *118*, 1906.
(8) (a) Shibayama, K.; Seidel, S. W.; Novak, B. M. *Macromolecules* **1997**, *30*, 3159. (b) Goodwin, A.; Novak, B. M. *Macromolecules* **1994**, *27*, 5520.
(9) All polymerizations were carried out in a drybox under an Ar atmosphere. Catalyst and monomer solutions were prepared immediately before use. In all cases, dichloro(η^5-cyclopentadienyl)(dimethylamido)titanium(IV) (**II**) was used as the catalyst. A typical polymerization procedure follows. Using volumetric glassware in the drybox, a 5.45 mM solution of **II** was prepared in toluene. A second 1.96 M toluene solution of (*R*/*S*)-*N*-(1-phenylethyl)-*N*′-methylcarbodiimide (**I**) was prepared similarly. Using syringes, 50 μL of the catalyst solution was added quickly to an ampule that contained 0.90 mL of the monomer solution and a stir bar. The ampule was sealed and the reaction solution allowed to stir at 30 °C over the course of several hours, during which time the solution would become increasingly viscous until the solutions would cease to flow. After complete reaction, the polymer was isolated by precipitation into methanol. Lyophilization from benzene yielded the poly-**I** as a fluffy white solid.
(10) Cotts, P. M.; Swager, T. M.; Zhou, Q. *Macromolecules* **1996**, *29*, 7323.
(11) Benoit, H.; Doty, P. *J. Phys. Chem.* **1953**, *57*, 958.
(12) Kratky, O.; Porod, G. *Recl. Trav. Chim.* **1949**, *68*, 1106.
(13) Tsvetkov, V. N. *Rigid-Chain Polymers; Hydrodynamic and Optical Properties in Solution*; Consultants Bureau: New York, 1989; pp 19−29.
(14) Fujita, H. *Polymer Solutions*; Elsevier: New York, 1990; pp 139−176.
(15) Yamakawa, H.; Stockmayer, W. H. *J. Chem. Phys.* **1972**, *57*, 2843.
(16) Norisuye, T.; Fujita, H. *Polym. J.* **1982**, *14*, 143.
(17) Murakami, H.; Norisuye, T.; Fujita, H. *Macromolecules* **1980**, *13*, 345.
(18) Yamakawa, H.; Fujii, M. *Macromolecules* **1973**, *6*, 407.
(19) Schmidt, M. *Macromolecules* **1984**, *17*, 553.
(20) Tsuji, T.; Norisuye, T.; Fujita, H. *Macromolecules* **1975**, *7*, 558.
(21) Shibayama, K.; Seidel, S. W.; Novak, B. M. *Macromolecules* **1997**, *30*, 3159.

MA9718006